A.B. SMIRNOV, O.S. LYTVYN, V.A. MOROZHENKO, R.K. SAVKINA, M.I. SMOLIY, R.S. UDOVYTSKA, F.F. SIZOV

V.E. Lashkaryov Institute of Semiconductor Physics, Nat. Acad. of Sci. of Ukraine
(41, Nauky Av., Kyiv 03028, Ukraine; e-mail: alex_tenet@isp.kiev.ua)

ROLE OF MECHANICAL STRESSES AT ION IMPLANTATION OF CdHgTe SOLID SOLUTIONS

The properties of n-$Cd_xHg_{1-x}Te/CdZnTe$ ($x \approx 0.223$) structures implanted with B^+ and Ag^+ ions with an energy of 100 keV to a dose of 3×10^{13} cm^{-2} are studied. The software package TRIM_2008 was applied to simulate the ion implantation process. The surface morphology of heterostructures and their optical, mechanical and electrical properties are studied. It is found that the ion irradiation of specimens gives rise to the formation of a characteristic relief on their surface, as well as a layer in the near-surface region, where the optical parameters differ from those in the matrix. The implantation of $Cd_xHg_{1-x}Te$ epitaxial layers with boron and silver ions with the same energy and to the same dose brings about the formation of a damaged layer, substantially non-uniform by the thickness and the damage character, with maximum mechanical stresses that differ by two orders of magnitude. The values of the crystal lattice contraction coefficient β and the mechanical stresses $\sigma_{\max}$ in the region of radiation-induced disordering in the solid solution are determined. The influence of mechanical stresses in the doped layer on the defect redistribution and the formation of properties of $Cd_{0.223}Hg_{0.777}Te$ after the implantation is discussed.

K e y w o r d s: ion implantation, nano-structurization, semiconductor structure.

1. Introduction

Strain fields that emerge at the crystal growth owing to both the mismatch between the crystal lattice constants in the epitaxial layer and the substrate and the difference between the corresponding coefficients of linear thermal expansion are an important factor governing the structural, optical, and electric properties of semiconducting hetero-epitaxial structures. An example of the efficient application of growth-induced strains is given by CMOS transistors, in which the substantial deformations in the channel region are obtained by combining strained Si and SiGe layers. As a result, the mobility of charge carriers increases [1, 2]. A substantial improvement of light-emitting characteristics is observed at low excitation levels for quantum wells fabricated on the basis of A_3B_5 compounds and compressively stressed in the heterojunction plane, which occurs owing to the creation of conditions for inverse level population [3]. A possibility to generate the powerful THz radiation in strained quantum-sized Si/SiGe structures is

also under discussion [4]. The application of strained layers allowed the transition to a novel class of three-dimensional nanostructures with strictly controlled dimensions and form (such as nanotubes and corrugated films) to be made [5].

Deformations that arise in heterostructures owing to external influences belong to a different type. For instance, the strain fields emerge due to the treatment of semiconducting materials and structures by fluxes of high-energy particles, ions, and atoms, as well as at their laser irradiation, ionic implantation, and so forth. The deformations control the transformation processes occurring in the system of impurities and defects in heterostructures and are responsible for their final physical properties. In particular, the implantation of oxygen and nitrogen to high doses (3×10^{18} cm^{-2}) followed by the annealing forms the basis for the creation of SIMOX and SIMON silicon structures with the so-called hidden dielectric oxynitride layers [6].

We found earlier that, when the substrate (Si) confines a deformation, the nonzero shear components of the strain tensor emerge in epitaxial CdHgTe films at various crystallographic orientations of the structure, which gives rise to a piezoelectric polarization of

Table 1. **Parameters of CdHgTe surface before and after implantation**

Specimen	Roughness parameters for a 1×1-μm^2 surface fragment		
	The area of real surface, μm^2	Area difference between the relief and the ideal surface*, %	Root-mean-square roughness R_q, nm
Initial	1.008	0.8	2.45
Implanted with boron	1.016	1.6	2.48
Implanted with silver	1.034	3.4	3.11

*Ideal surface is absolutely flat with an area of 1 μm^2.

the material [7]. This effect serves as a basis for the efficient application of multilayered CdHgTe/Si heterostructures to detect infra-red (IR) radiation making no use of electric bias and cooling [8]. In other words, we may assert that the research of regularities in the processes that occur in deformed heterostructures on the basis of CdHgTe is interesting and challenging from the practical viewpoint.

This work aimed at studying the influence of low-energy irradiation with B$^+$ and Ag$^+$ ions, as well as implantation-induced mechanical stresses, on the properties of hetero-epitaxial CdHgTe/CdZnTe structures. The consideration of this issue is actual and important for the development of modern vision systems in the IR spectral intervals of 3–5 and 8–12 μm on the basis of CdHgTe heterostructures [9].

2. Experimental Technique

Systematic studies of the structural, optical, and electric properties of semiconductor heterostructures n–$Cd_x Hg_{1-x}Te$/CdZnTe ($x \approx 0.223$) before and after their implantation are carried out. In addition, the mathematical simulation of the process of ion implantation was done with the use of the software package *TRIM_2008*.

The specimens to study were divided into two groups. The specimen in the first and second groups were irradiated with B$^+$ and Ag$^+$ ions, respectively. The structures were irradiated from the CdHgTe film side on a *Vezuvii* implanter. The implantation energy was equal to 100 keV and the implantation dose to $Q = 3 \times 10^{13}$ cm^{-2} for both groups. After the implantation, all specimens were held for 5 h at 75 °C in the Ar atmosphere with an excess pressure of 4 Pa in the chamber [10].

The surface state of the examined specimens was monitored with the help of atomic force microscopy (AFM). Their optical parameters were determined on a laser ellipsometer *LEF-2M-1* at the wavelength $\lambda = 628.3$ nm. The refractive index n and the extinction coefficient k of initial specimens corresponded to standard literature data for CdHgTe [11]. The chemical content x of $Cd_x Hg_{1-x}Te$ solid solution was determined from the transmission spectra [12] measured on a Fourier spectrometer *Infralum FT-801* with a resolution of 2 cm^{-1} in a spectral interval 3 to 14 μm. The mechanical properties of CdHgTe films were found with the use of a *Shimadzu HMV-2000* microhardness tester.

To carry out the electrophysical researches, a mesostructure was fabricated by the chemical etching of the specimens in a standard etching solution Br–HBr. The dark resistances of all specimens at room temperature were within the interval $R = (10 \div 20)$ Ω. The concentration and the mobility of majority charge carriers were determined following the van der Pauw method at the temperature $T = 78$ K in the magnetic field interval from 0.05 to 0.5 T. The capacitance parameters were obtained on a precision device *LCR-819* in the temperature interval 78–300 K.

3. Experimental Results

3.1. Surface topometry

It was found that the ion irradiation of the surface of studied specimens gives rise to the formation of a characteristic relief on it. The AFM images of the initial surface of typical heterostructure specimens on the basis of CdHgTe (Figs. 1,*a* and 2,*a*) demonstrate a grid of quasipores $(3.5 \div 10)$ nm in depth and $(50 \div 160)$ nm in diameter, as well as closely packed grains ranging from 40 to 80 nm in dimensions and located in
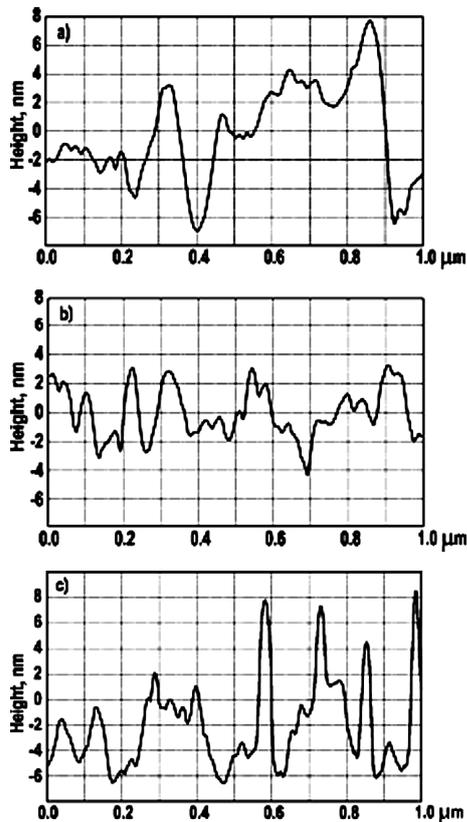
Fig. 1. Profile of $Cd_xHg_{1-x}Te$ ($x \approx 0.223$) surface (*a*) before implantation and after implantation with (*b*) boron and (*c*) silver

Fig. 2. AFM images of $Cd_{0.223}Hg_{0.777}Te$ surface (*a*) in the initial state, (*b*) after implantation with B^+, and (*c*) after implantation with Ag^+

the surface plane between the pores. The root-mean-square roughness over a surface fragment 1×1 μm^2 in area amounts to 2.45 nm.

Implantation with boron results in insignificant changes of the surface relief (Figs. 1, *b* and 2, *b*). Namely, the ordered grid of quasipores is not observed, but the surface became denser: keeping the same roughness parameters, its area increased (see Table 1). Some grains (their sizes did not change in comparison with those on the initial surface) formed chains with grooves between them with a depth of up to 10 nm. At the same time, the implantation with silver ions gives rise to the emergence of a uniform array of nano-islands 5 to 25 nm in height and with a base diameter of 13 to 35 nm against the background of the insignificant smearing of initial grain boundaries and the constant surface porosity (Fig. 1,*c* and 2,*c*). Accordingly, the relief became more de-
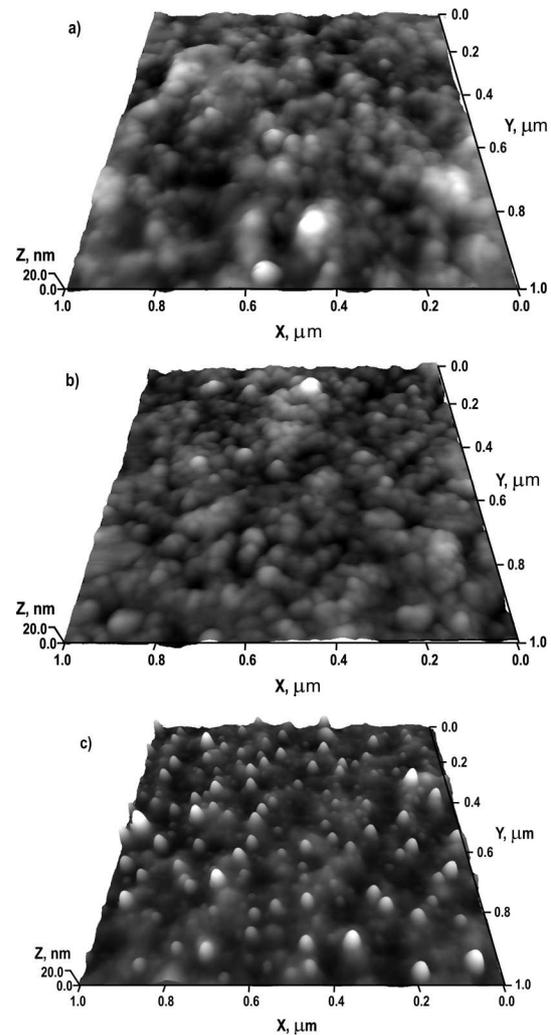
veloped, and the root-mean-square roughness R_q increased (Table 1).

3.2. Optical Parameters

While interpreting the ellipsometric data for the determination of optical parameters for the specimens in the first group, a two-layer model of the refracting system, namely damaged layer/CdHgTe/CdZnTe, was engaged [13]. For the specimens in the second group, the interpretation of the results obtained and the determination of the optical parameters in the damaged layer became possible only after having

Table 2. **Parameters of the optical system "damaged layer"/Cd$_{0.223}$Hg$_{0.777}$Te;**
d, d_1, and d_2 are the thicknesses of a CdHgTe film in the initial state and the damaged layers
formed after implantation; n, n_1, n_2 and k, k_1, k_2 are the refractive indices and the extinction
coefficients of the CdHgTe film in the initial state and the damaged layers

CdHgTe film in the initial state $d = 17.4~\mu$m $n = 3.87$; $k = 1.1$	"Damaged layer"/CdHgTe		
	d_1/d_2, μm	Optical parameters	
		$n_1/n_2/n$	$k_1/k_2/k$
Implantation with B$^+$	0.38/–	1.029/–/3.56	0.098/–/0.67
Implantation with Ag$^+$	0.048/0.056	1.7/1.38/3.5	0.06/0.09/1.19

made the system more complicated by introducing an additional layer, which is associated with a specific character of damages in CdHgTe induced by silver ions. The values of refractive indices and extinction coefficients in the damaged layers turned out anomalously small [14] with respect to the corresponding values for CdHgTe in both groups of specimens. For typical specimens, the values of optical parameters $n_{1,2}$ and $k_{1,2}$, and the thicknesses of damaged layers $d_{1,2}$ are quoted in Table 2. Damages revealed in the near-surface region of CdHgTe form a layer not thicker than 0.4 or 0.1 μm in the case of implantation with boron or silver, respectively.

The optical transmission spectra of the examined specimens are shown in Fig. 3. The average transmittance T for all specimens in the initial state amounted to about 50%. A characteristic feature of the spectrum for the Cd$_x$Hg$_{1-x}$Te solid solution with $x \approx 0.223$ is the presence of the absorption edge at $\lambda_1 = 6.60$ μm. After the thermal treatment, the transmittance for the first group of structures (only!) decreased down to 10% in the whole spectral interval, and an additional absorption interval emerged with the cut-off at $\lambda_2 = 9.94$ μm.

3.3. Mechanical properties

The variation of the relative microhardness was determined by the formula

$$\eta = \frac{HV_1}{HV}, \qquad (1)$$

where HV_1 and HV are the microhardnesses of specimens before and after the implantation, respectively. The researches showed that, after the implantation
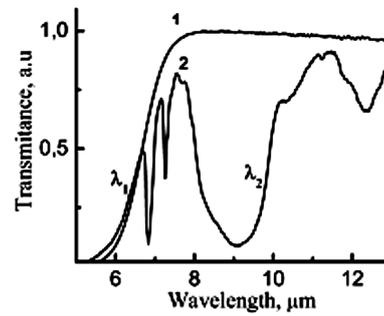
Fig. 3. Transmission spectra of a typical Cd$_{0.223}$Hg$_{0.777}$Te/CdZnTe specimen (*a*) in the initial state and (*b*) after implantation with boron and annealing

and the annealing of the specimens, the microhardness grew (up to $\eta = 1.12$) for the specimens implanted with boron and a little decreased ($\eta = 0.96$) for the specimens implanted with silver in comparison with the reference value ($\eta = 1$).

3.4. Electrical properties

The analysis of the magnetic-field dependences of the Hall coefficient R_H and the conductivity σ showed that the epitaxial CdHgTe film has the conductivity of the n-type in the initial state. The character of the dependences $R_H(B)$ and $\sigma(B)$ can be explained by the presence of electrons of two types (as was done in work [15]): with low ($\mu_{n_1} = 0.322$ m^2/V$\cdot$s) and high ($\mu_{n_1} = 8.0$ m^2/V$\cdot$s) mobilities. After the implantation, the concentration of electrons with a low mobility increased from $n_1 = 4.0 \times 10^{21}$ m^{-3} to $n_{(B^+)} \approx 6 \times 10^{22}$ m^{-3} in the CdHgTe specimens implanted with boron and to $n_{(Ag^+)} \approx 1.5 \times 10^{22}$ m^{-3} in the specimens implanted with silver ions. No contribution of high-mobility electrons, the concen-
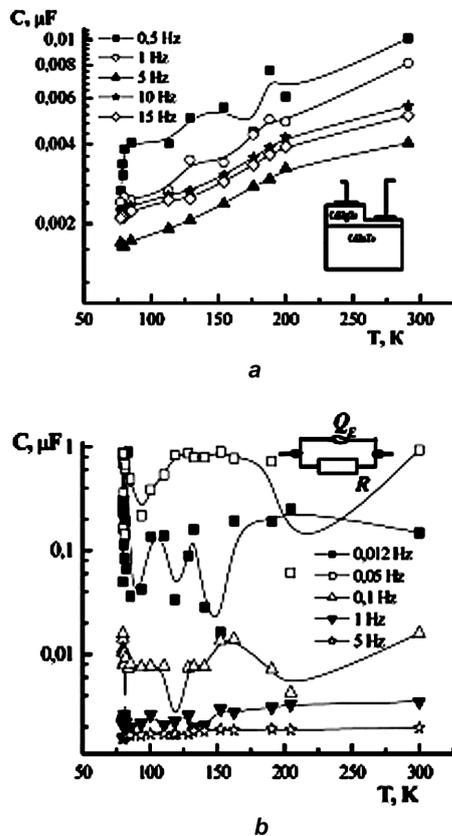
Fig. 4. Temperature dependences of the capacitance of typical $Cd_{0.223}Hg_{0.777}Te/CdZnTe$ structures implanted with (*a*) B^+ and (*b*) Ag^+ and measured at various frequencies of the excitation signal. The inset in panel (*a*) demonstrates the scheme of the examined mesostructure fabricated with the use of the method of chemical etching, and the inset in panel (*b*) shows the corresponding equivalent circuit

tration of which in the initial state was equal to $n_2 \approx 5.0 \times 10^{18}$ m^{-3}, was revealed for all specimens after their treatment.

In Fig. 4, the temperature dependences of the capacitance in the frequency interval from 10 to 10^4 Hz are depicted for both groups of specimens. The heterostructures implanted with silver were found to response to an applied external electric field starting from frequencies much lower than 12 Hz (Fig. 4, *a*), in contrast to the specimens implanted with boron. The inset in Fig. 4, *a* demonstrates the physical scheme and the inset in Fig. 4, *b* the equivalent electric circuit of the examined structures. Taking the non-uniform distribution of microscopic properties in the implanted material into account, a nonlinear

constant-phase element was introduced to describe the resistive and capacitive properties of the structure [16]. This element is designated as Q_E on the circuit diagram. Its impedance is described by the relation $Z_{QE} = (A_0(j\omega)^n)^{-1}$, where A_0 is an independent factor, ω is the frequency, and $n_{n.i.}$ is a parameter of nonideality for the capacitor of this type, which varies within the limits $-1 \le n_{n.i.} \le 1$.

4. Discussion

Ion implantation is widely used to manufacture IR photodiodes on the basis of CdHgTe solid solutions. Instrument structures on the basis of *n*-type layers located in the near-surface region of *p*-CdHgTe are usually obtained by implanting B^+ ions into the target. To obtain *p–n* transitions, CdHgTe of the *n*-type is implanted with As^+ ions [11, 17].

At the same time, the implantation of semiconductor hetero- and homo-epitaxial systems with high-energy ions is known to be accompanied by the insertion of a considerable number of defects [18, 19]. The kinetics of this process is driven by the diffusion mobility of defects and depends on both the presence of migration barriers and the character of the interaction between doping elements, impurities, and intrinsic point defects in the semiconductor. On the other hand, the internal mechanical stresses in the regions of radiation-induced disordering violate the uniformity of physical characteristics in the semiconductor material, which allows regions with special properties, e.g., getter ones, to be formed in the target [20–23]. The results of experimental works [21–23] testify that the redistribution of radiation-induced defects also takes place at the ion irradiation of semiconductor materials in the energy interval 100–150 keV.

Consider the processes occurring in CdHgTe solid solutions at their irradiation with 100-keV ions. It is well-known that this substance reveals a substantial sensitivity to technological processes. It is especially true for the Hg–Te sublattice, because the enthalpy of Hg-Te bond formation is low ($\Delta H_f = 0.33$ eV) in comparison with that for the Cd-Te bond ($\Delta H_f = 1.044$ eV) [24]. The mathematical simulation of the process of ion implantation with the use of the software package *TRIM_2008* allowed the parameters of the radiation-induced disordering region to be determined for the cases of irradiation with 100-keV boron and silver ions; the corresponding values are listed

in Table 3. The energy losses (the energy transmitted by an implanted ion to the nuclear subsystem of the target by means of elastic interactions) amount to 79.2 eV/Å for B^+ ions and 27.68 eV/Å for Ag^+ ones. Therefore, we may assert that the track of a single ion (B^+ or Ag^+) forms a region around it in the CdHgTe target, where the crystal structure of the semiconductor is considerably damaged. The near-surface region of the target becomes saturated with point defects. In particular, in CdHgTe solid solutions, these are vacancies and mercury interstitial sites [25]. Mercury interstitial sites, Hg_i, are also formed owing to the penetration of implanted atoms into the cation sublattice of the semiconductor crystal matrix.

The boundaries of the CdHgTe crystal lattice distortion are given by the implant distribution profile $C(z)$. In Fig. 5, the corresponding distributions calculated for the implantation with boron and silver are shown. The impurities are mainly located in the near-surface region of the epitaxial CdHgTe layer 0.4\0.1 μm in thickness. The concentration of ions reaches its maximum value of about 10^{24} m^{-3} at a depth of 0.2\0.05 μm. At $z \rightarrow 0.4$\0.1 μm, the concentration of the introduced impurity $C(z)$ decreases by an order of magnitude. It should be noted that the thickness of a damaged layer determined from the results of ellipsometric measurements (of about 0.38\0.1 μm, see Table 2) is close to the thickness of the layer, in which the maximum implant concentration is observed (Fig. 5).

Radiation-induced defects distort the crystal lattice and, accordingly, the heterostructure. The magnitude of mechanical stresses created in the CdHgTe film after its implantation can be determined from the relation [26]

$$\sigma(z) = \frac{C(z)\beta E}{(1-\nu)}, \qquad (2)$$

where ν is Poisson's ratio, E is the Young modulus, z is the coordinate, and $C(z)$ is the distribution profile of an impurity introduced into the target. The coefficient of CdHgTe crystal lattice contraction by the introduced implant, β, was determined using the results of X-ray diffraction studies of specimens and amounts to $\beta = 3.51 \times 10^{-31}$ m^3 for silver and 1.25×10^{-32} m^3 for boron. Therefore, the mechanical stresses that arise in the near-surface layer of an epitaxial CdHgTe film attain, according to our estimations, the maximum values of $\sigma_{max} \approx 1.4 \times 10^3$ Pa for boron and
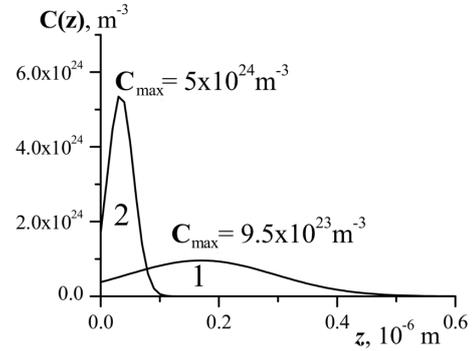

Fig. 5. Profiles of implant distribution in typical $Cd_xHg_{1-x}Te/CdZnTe$ ($x \approx 0.223$) structures implanted with (*1*) boron and (*2*) silver ions
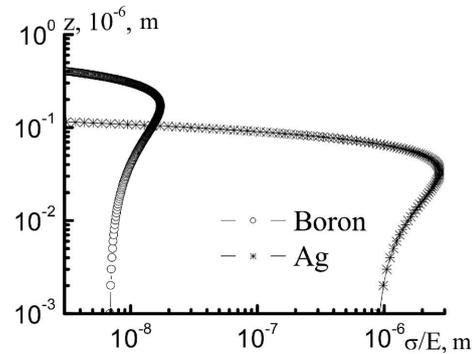

Fig. 6. Profiles of deformations in the $Cd_{0.223}Hg_{0.777}Te$ film on the CdZnTe substrate induced by introducing the B^+ and Ag^+ impurities

Table 3. **Parameters of the CdHgTe region subjected to the ion-induced disordering**

Parameters	B^+	Ag^+
Path projection R_p, μm	0.22	0.0365
Straggling, μm	0.17	0.024
Maximum mechanical stresses σ, Pa	1.4×10^3	2.2×10^5
Maximum impurity concentration C, m^{-3}	9.5×10^{23}	5.0×10^{24}
Vacancy concentration C_v, N/Å ion	20.0	4.5

$\sigma_{max} \approx 2.2 \times 10^5$ Pa for silver. If the contribution of intrinsic defects is taken into account, expression (2) looks like

$$\sigma_x = \sigma_y = -2E\frac{1}{\Omega}(\delta V_V C_V + \delta V C), \qquad (3)$$

where σ_x and σ_y are the components of normal stresses, Ω is the atomic volume of the crystal lattice, δV_V and δV are the relaxation volumes of a point defect and an impurity, respectively, and the values of C_V and C are given in Table 3. In Fig. 6, the diagrams of the residual concentration-induced stresses as functions of σ/E are plotted. Hence, the implantation of epitaxial CdHgTe layers with boron or silver ions, which is characterized by the same energy and the same dose, results in the formation of damaged layers that are considerably different in those two cases by the character of damages and the thicknesses of damaged layers, with the maxima of the corresponding mechanical stresses differing by two orders of magnitude.

In our opinion, the distinction between effects arising in the near-surface layer of an epitaxial CdHgTe film owing to its treatment with boron and silver ions is connected with the opposite character of deformations inserting by those ions into the crystal lattice. Really, as was shown in work [27], the implantation of CdHgTe with ions of small radius (such as B^+ with a radius of 1.17 Å [28]) stimulates the contraction of the damaged layer, whereas the implantation of this material with Hg ions with a radius of 1.76 Å [28] or Cd ones with a radius of 1.71 Å [28] (in our case, are these are Ag ions with a radius of 1.75 Å [28]), on the contrary, gives rise to the stretching of the semiconductor near-surface layer. Hence, the squeezing or stretching of the near-surface region in the epitaxial CdHgTe film and, respectively, the stretching or squeezing of deeper layers in this material (i.e. the appearance of a strain gradient) promotes the redistribution of point defects over the system, as the heterostructure is annealed.

It should be noted that the final distribution of defects in implanted structures depends not only on the treatment regimes and the properties of ions used for the implantation. Impurities, being introduced into CdHgTe, demonstrate a high ability to penetrate, but not the chemical activity [14]. The intrinsic defects in CdHgTe are also characterized by a high diffusion mobility, e.g., along prolonged defects. This means that the diffusion, in the presence of deformation gradient, changes the final distribution of defects in the implanted CdHgTe-based heterostructure with the help of the deformation-assisted drawing out of migrating atoms.

Taking into account that mercury and boron are driven by the vacancy mechanism, whereas silver moves, being governed by the dissociative mechanism, the migration of interstitial mercury atoms, Hg_i, was found to be the dominating process in the specimens. In this case, the flow of defects is directed normally to the specimen surface, from the contracted region to the stretched one. At the same time, the redundant pressure in the chamber prohibits mercury from moving toward the epitaxial film surface [29] during the annealing of the specimen.

Hence, in the course of annealing of the specimens implanted with boron, interstitial mercury diffuses mainly into the specimen depth, where the "healing" of intrinsic defects – mercury vacancies V_{Hg} – takes place, which results in an enhancement of the electron contribution to the conductivity in CdHgTe. This conclusion is favored by the variations in the electrophysical parameters, in particular, by a growth of the electron concentration (see Section 3.4). The topometric results demonstrate the effect of surface compaction for the specimens in the first group after their implantation and annealing. This fact can be explained by the process of vacancy-assisted dissolution of nano- and micropores, which evidently brings about the strengthening of the surface of the treated material [30]. During this process, both the translational motion of grains and the shear macrodeformation are directed along the intergrain boundaries, whereas the process of surface "healing" in the directions perpendicular to that of grain shifts. In such a way, the mechanical stresses relax, and the disordered semiconductor layer changes its porous structure. The opposite character of a deformation in the near-surface layers of specimens implanted with silver does not promote, evidently, the pore disappearance and impedes mercury to diffuse into the target depth at the annealing. Moreover, the stretching of the near-surface region in the epitaxial CdHgTe film and, accordingly, the contraction of deeper layers may be the origin of drawing out silver ions onto the surface. The formation of a uniform array of nanoislands can be associated with silver's liability to create solid solutions in CdHgTe at the ion implantation [14] and with the extraction of Ag in the form of nanoparticles in the target [31]. Another possible explanation consists in the extraction of Te precipitates from the anion sublattice of CdHgTe [32].

At last, let us analyze the results obtained for the capacitive response of the examined structure to a sinusoidal electric driving signal generated by an LCR-meter. The character of the obtained temperature and frequency dependences of the capacity of the studied specimens (see Fig. 4) depends on whether the charge transfer process is quick enough to trace the oscillations of the alternating voltage applied to the structure and used to carry out CV measurements.

The features observed at low frequencies testify to the process of electric charge transfer associated with the ion migration. From the frequency dependences and with the help of the relation $f_{\max}\tau_M = 1$ [16], the relaxation times of the conductivity in the specimens, τ_M, were determined. The τ_M-values were found to fall within the interval from 0.3 ms (specimens of the first group) to 30 ms (specimens of the second group). A certain analogy can be made with the ion-migration polarization in insulators, which originates from the presence of layers with different conductivities in the material [33].

For the results obtained in this work to be successfully interpreted, some refinements should be made to both the analog and physical models. In addition, X-ray diffraction researches of the specimens should be carried out, which would allow the mechanism of charge transfer in a disordered system – such as the CdHgTe solid solution subjected to the irradiation with boron and silver ions – to be elucidated.

5. Conclusions

1. Irradiation of the specimens of $Cd_{0.223}Hg_{0.777}Te/$CdZnTe heterostructures with 100-keV B^+ and Ag^+ ions to an implantation dose of 3×10^{13} cm^{-2} gives rise to the specimen surface structurization.

2. The processes of ion penetration and interaction of point defects with the porosity is accompanied by irreversible changes in the structure-sensitive properties of the examined heterostructures on the basis of CdHgTe. The formation of layers with the optical parameters n and k that are anomalously small in comparison with the corresponding matrix values was revealed in the near-surface region of CdHgTe film.

3. It was found that, when CdHgTe is implanted with boron ions, its crystal lattice becomes squeezed. In the case of the implantation with ions of larger radius (Ag^+), the stretching of the CdHgTe crystal lattice takes place.

4. The coefficient of crystal lattice contraction β for the CdHgTe solid solution was found to equal 3.51×10^{-31} m^3 and 1.25×10^{-32} m^3 in the cases of the implantation with boron and silver, respectively. The maximal mechanical stresses $\sigma_{\max}$ in the region of radiation-induced disordering were determined to equal about 1.4×10^3 Pa for the boron implantation and about 2.2×10^5 Pa for the silver one.

5. The penetration of ions changes the mechanical characteristics of the epitaxial layer of the narrow-band semiconductor. The deformation resistance of a CdHgTe film depends on the atomic radius of an implant, namely B^+ ions increase and Ag^+ ones reduce it.

1. D. Paul, Semicond. Sci. Technol. **19**, 75 (2004).
2. A.A. Orouji and M.J. Kumar, Superlatt. Microstruct. **39**, 395 (2006).
3. A.D. Bondarev, D.A. Vinokurov, V.A. Kapitonov *et al.*, Pis'ma Zh. Tekhn. Fiz. **24**, 46 (1998).
4. M.S. Kagan, I.V. Altukhov, E.G. Chirkova, V.P. Sinis, R.T. Troeger, S.K. Ray, and J. Kolodzey, Phys. Status Solidi B **235**, 135 (2003).
5. V.Ya. Prinz, Physica E **24**, 54 (2004).
6. W.B. Li, E.X. Zhang, M. Chen, N. Li, G.Q. Zhang, and Z.L. Liu, Semicond. Sci. Technol. **19**, 571 (2004).
7. A.B. Smirnov, Semicond. Phys. Quant. Electr. Optoelectr. **15**, 170 (2012).
8. T. Kryshtab, R. Savkina, F. Sizov, A. Smirnov, M. Kladkevich, and V. Samoylov, Phys. Status Solidi C **9**, 1793 (2012).
9. F.F. Sizov, *Photoelectronics for Vision Systems in Invisible Spectral Intervals* (Akademperiodika, Kyiv, 2008) (in Russian).
10. A.B. Smirnov, R.K. Savkina, R.S. Udovitskaya, A.Z. Evmenova, and F.F. Sizov, Sensor Electr. Microsyst. Technol. **3**, N 9, 62 (2012).
11. A. Rogalski, *Infrared Detectors* (CRC Press, Boca Raton, 2010).
12. V.V. Tetyorkin, Z.F. Icasiv, and F.F. Sizov, Ukr. Fiz. Zh. **44**, 1128 (1999).
13. F.F. Sizov, N.I. Klyui, A.N. Luk'yanov, R.K. Savkina, A.B. Smirnov, and A.Z. Evmenova, Techn. Phys. Lett. **34**, 377 (2008).
14. M.I. Ibragimova, V.Yu. Petukhov, and I.B. Khaibullin, Fiz. Tekh. Poluprovodn. **27**, 560 (1993).

15. R.K. Savkina, A.B. Smirnov, and F.F. Sizov, Semicond. Sci. Technol. **22**, 97 (2007).

16. Z.B. Stoinov, B.M. Grafov, B. Savova-Stoinova, and V.V. Elkin, *Electrochemical Impedance* (Nauka, Moscow, 1991) (in Russian).

17. *Mercury Cadmium Telluride: Growth, Properties and Applications*, edited by P. Capper and J.W. Garland (Wiley, London, 2011).

18. K.D. Mynbaev and V.I. Ivanov-Omskiy, Semiconductors **40**, 1 (2006).

19. L.S. Smirnov, *Problems of Semiconductor Radiation Technology* (Nauka, Novosibirsk, 1980) (in Russian).

20. V.G. Litovchenko and B.N. Romanyuk, Fiz. Tekh. Poluprovodn. **1**, 150 (1983).

21. V.A. Uskov, A.A. Krasnov, and V.A. Ivanov, in *Proceedings of the 6-th All-Union Conference on Gallium Arsenide Researches* (Tomsk, 1987), Vol. 2, p. 134 (in Russian).

22. P.N. Krylov and A.A. Lebedev, Vestn. Udmursk. Univ. **4**, 29 (2006).

23. P.N. Krylov, Yu.V. Rats, and A.L. Sterkhov, Vestn. Nizhegorod. Gos. Univ. Ser. Fiz. Tverd. Tela **2**, 79 (1998).

24. V.B. Lazarev, *Physical and Chemical Properties of Semiconductor Substances* (Nauka, Moscow, 1979) (in Russian).

25. S. Holander-Gleixner, B.L. Williams, H.G. Robinson, and C.R. Helms, J. Electron. Mater. **71**, 692 (1997).

26. A. Cerutti and C. Ghezzi, Phys. Status Solidi A **17**, 273 (1973).

27. H. Ebe, M. Tanaka, and Y. Miyamoto, J. Electron. Mater. **28**, 854 (1999).

28. R.A. Lidin, L.L. Andreeva, and V.A. Molochko, *Constants of Inorganic Substances* (Begell House, New York, 1995).

29. C.R. Helms, J. Vac. Sci. Technol. A **8**, 1178 (1990).

30. L.S. Palatnik, P.G. Cheremskoi, and M.Ya. Fuks, *Pores in Films* (Energoizdat, Moscow, 1982) (in Russian).

31. A. Meldrum, R. Lopez, R.H. Magruder *et al.*, Appl. Phys. **116**, 255 (2010).

32. J.D. Benson, J.B. Varesi, A.J. Stoltz, E.P.G. Smith, S.M. Johnson *et al.*, J. Electron. Mater. **35**, 1434 (2006).

33. E.V. Stukova, A.Yu. Milinskii, and V.V. Maslov, Izv. Ross. Gos. Pedagog. Univ. **95**, 58 (2009).

О.Б. Смірнов, О.С. Литвин,
В.О. Мороженко, Р.К. Савкіна, М.І. Смолій,
Р.С. Удовицька, Ф.Ф. Сизов

РОЛЬ МЕХАНІЧНИХ НАПРУЖЕНЬ ПРИ ІОННІЙ ІМПЛАНТАЦІЇ ТВЕРДИХ РОЗЧИНІВ CdHgTe

Р е з ю м е

Представлено результати систематичних досліджень структурних, оптичних та електричних властивостей напівпровідникових гетероструктур n-$Cd_x Hg_{1-x} Te$/CdZnTe ($x \sim 0{,}223$) до та після опромінення іонами B^+ та Ag^+ (100 кеВ, доза імплантації $Q = 3 \cdot 10^{13}$ см$^{-2}$). Здійснено математичне моделювання процесу іонної імплантації із застосуванням програмного пакета TRIM_2008. Встановлено, що в результаті опромінення на поверхні досліджуваних зразків відбувається утворення характерного рельєфу, а в приповерхневій області – шару з відмінними від матриці оптичними характеристиками. В результаті імплантації епітаксійних шарів $Cd_x Hg_{1-x} Te$ іонами бору та срібла з однаковою енергією та дозою утворюється суттєво відмінний за характером пошкодження та товщиною порушений шар з максимальними механічними напруженнями, що відрізняються на два порядки величини. Отримано значення коефіцієнта стискання β кристалічної ґратки та механічних напружень $\sigma_{макс}$ в області радіаційного розупорядкування твердого розчину. Обговорюється роль механічних напружень легованого шару у перерозподілі дефектів і формуванні постімплантаційних властивостей $Cd_{0{,}223} Hg_{0{,}777} Te$.